Aerosol and Air Quality Research, 12: 8–19, 2012
Copyright © Taiwan Association for Aerosol Research
ISSN: 1680-8584 print / 2071-1409 online
doi: 10.4209/aaqr.2011.08.0133

Variability of Urban Aerosols over Santiago, Chile: Comparison of Surface PM_{10} Concentrations and Remote Sensing with Ceilometer and Lidar

Ricardo C. Muñoz[1*], Ricardo I. Alcafuz[2]

[1] *Department of Geophysics,University of Chile, Av. Blanco Encalada 2002, 4th Floor, Santiago, Chile*
[2] *Dirección Meteorológica de Chile, Av. Portales 3450, Estación Central, Santiago, Chile*

ABSTRACT

Lidar instruments have proven useful for characterizing the structure and dynamics of aerosol layers. We compare here the diurnal, seasonal and vertical variability of urban aerosols as described by a lidar ceilometer and surface particulate matter (PM_{10}) concentrations using 4 years of observations available at Santiago, Chile, a city having a serious PM_{10} air pollution problem. Large diurnal variation of ceilometer backscatter values is observed on average up to 600 m (400 m) above the surface in spring and summer (fall and winter). The diurnal cycles of near-surface ceilometer backscatter and PM_{10} concentrations show prominent morning peaks. The large PM_{10} evening peak is less marked in the ceilometer backscatter values, suggesting that this significant feature of Santiago's air pollution is constrained to a shallow atmospheric layer. Daily averages of PM_{10} concentrations and ceilometer backscatter have correlations of 0.5 for the full data set, and a maximum of 0.75 for April. Results are supplemented with recently available observations gathered with a 355 nm elastic lidar. While the smaller blind region of the ceilometer provides a more complete picture of the aerosol layer dynamics, the higher resolution of the lidar allows a better definition of the aerosol layer structure. Both instruments suggest the frequent development of complex aerosol layers appearing over Santiago during the evening transition. The lidar shows also frequent occurrence of buoyancy oscillations in the stable basin's air mass.

Keywords: Aerosols; Lidar; Ceilometer; PM_{10}; Santiago; Chile.

INTRODUCTION

Considered as tracers of the airflow, aerosols provide valuable information on the dynamics and degree of mixing of the atmospheric boundary layer (ABL). Considered as air pollutants, on the other hand, they define environmentally problematic regions in terms of high concentration or high emission of particulate matter. For both applications, observation of the time/space distribution of aerosols in the ABL is of great interest. The lidar remote sensing technique has proven well suited for this task (Kovalev and Eichinger, 2004; Emeis, 2011). By emitting high-frequency laser pulses and measuring signal returns, lidars provide qualitative and quantitative information on aerosol distribution with high temporal and spatial resolution. With the transit from development-stage to commercially-available instruments, the number of reports on lidar applications in air pollution and ABL problems has increased steadily in the last few years. They have been variously applied to describe ABL dynamics and estimate its height (Cohn and Angevine, 2000; Martucci *et al.,* 2007; De Wekker and Mayor, 2009; McKendry *et al.,* 2011), as well as to characterize aerosols in the ABL and the lower troposphere (Papayannis *et al.,* 2007; McKendry *et al.,* 2009; Ponczkowsca *et al.,* 2009). One particular class of lidar deserves special mention. Although initially conceived as instruments for automatic cloud base measurements, lidar ceilometers have been shown to describe ABL aerosol layers during cloud-free conditions quite well (Eresmaa *et al.,* 2006; Münkel *et al.,* 2007; Sundström *et al.,* 2009; Van der Kamp and McKendry, 2010a).

Application of lidars to probe the ABL of Santiago basin in Chile is of special interest for two reasons. In first place, Santiago's particulate matter (as measured, for example, by the concentration of aerosols with aerodynamic size less than 10 μm, PM_{10}) constitutes a very serious air pollution problem. In fact, although according to its population (~6 Million inhabitants) Santiago cannot be properly considered a megacity, Molina and Molina (2004) included it as a case example for illustrating the most complex urban air pollution problems in the world. Fig. 1 puts Santiago's PM_{10} problem in the context of 16 cities in America considered in the Air Pollution section of the last World Bank Development Index report (World Bank, 2010). Santiago stands out for having one of the highest annual mean PM_{10}

* Corresponding author. Tel.: 56-2-978-4305;
Fax: 56-2-696-8686
E-mail address: rmunoz@dgf.uchile.cl

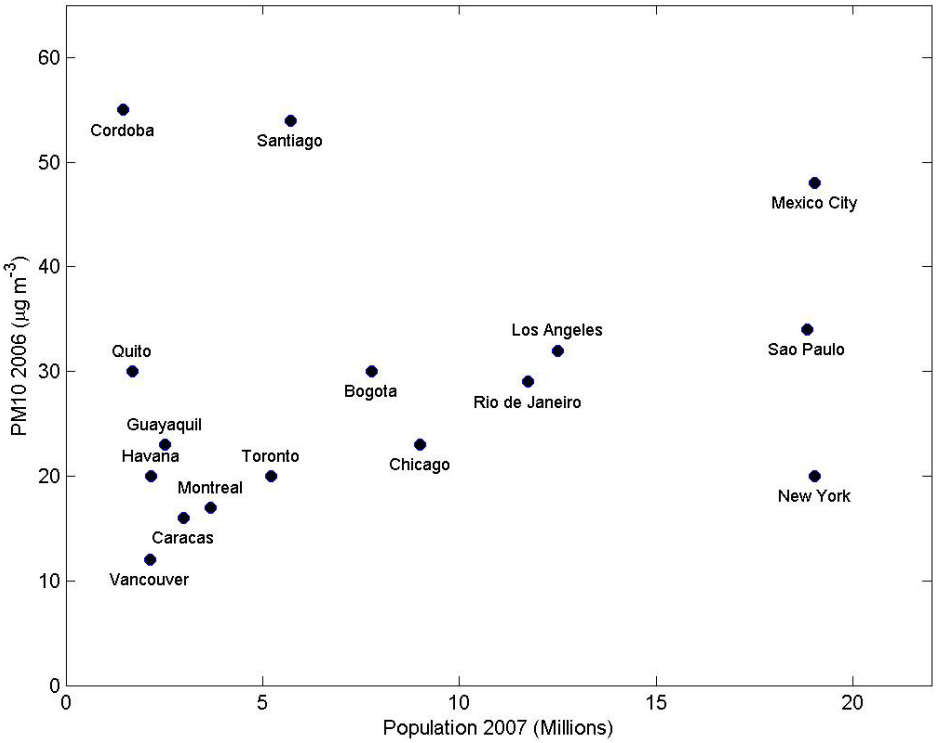

Fig. 1. Mean PM_{10} concentrations in 2006 and population in 2007 for 16 cities in America according to Table 3.14 (Air Pollution) in World Bank (2010).

concentrations, with a relatively small population. Being the national capital, considerable effort has been put along the years in reducing the problem through, for example, strict vehicle emission standards and public transportation fleet renewal. Its persistence, however, points to its severe climatic and geographical constraints (Rutllant and Garreaud, 1995; Romero *et al.,* 1999). Up to now, the extent of Santiago's PM_{10} problem has been characterized through a rather comprehensive air-quality monitoring network. While this information is what is needed to assess people's exposure, its near-surface character considerably limits its applicability for understanding the dynamics of the aerosol layers responsible for high impacts near the surface. Thus, lidar-derived vertical characterization of Santiago aerosols opens a new dimension to a better understanding of its air pollution problem. In second place, lidar characterization of aerosol dynamics in Santiago basin should provide very much needed information about various physical phenomena occurring in this complex terrain ABL. Despite its importance, Santiago lacks routine upper-air meteorological measurements performed in the basin. The closest aerological station (Santo Domingo) is located at the coast, about 100 km to the west of Santiago. While above 2000–3000 m above ground level (AGL) limited-scope comparisons suggest relatively good correlation between winds and temperature measured at Santo Domingo and Santiago, the situation is quite different in the lower layers due to the topographical confinement of the basin (Muñoz and Corral, 2011). Thus, topographically-driven low-level circulations like nocturnal katabatic flows or diurnal valley-mountain flows have been heretofore only hypothesized based on limited data analysis and numerical modeling (Schmitz, 2005; Saide *et al.,* 2011), but not yet fully observed or documented.

The present paper describes observations gathered in Santiago basin with two lidar instruments available only recently. The first one is a lidar ceilometer that has been in operation at the Department of Geophysics (DGF) of the University of Chile almost continuously since 2007 near downtown Santiago. The second one is a more advanced elastic lidar operating semi-continuously since May 2011 at the Chilean Weather Service (DMC) headquarters. These two instruments are beginning to provide a new look at Santiago's air pollution problem and ABL dynamics, part of which we attempt to describe here. More specifically, the objectives of the paper are: 1) to use the more extended ceilometer data to provide a first description of the diurnal/seasonal variation of the vertical distribution of aerosols over Santiago, 2) to explore the quantitative statistical relationship between ceilometer backscatter profiles and PM_{10} concentrations measured in Santiago, 3) to compare ceilometer and lidar observations, and 4) to describe some physical phenomena that lidar observations are beginning to uncover in Santiago's ABL. The second objective has been addressed before in other settings by Münkel *et al.* (2004; 2007), and van der Kamp and McKendry (2010b). Ceilometer-lidar comparisons in the third objective, on the other hand, have been presented also by McKendry *et al.* (2009), Heese *et al.* (2010), and Tsaknakis *et al.* (2011). More generally, the current work fits in recent efforts aiming at producing a more detailed characterization of the variability of aerosols in urban environments (e.g. Baxla *et al.,* 2009; Rana *et al.,* 2009).

DATA AND INSTRUMENTS

Particulate Matter Concentrations

Fig. 2 shows the urban area of Santiago and the location of the six PM_{10}- monitoring stations considered in this study. They measure hourly PM_{10} concentrations since 1997, and are subject to high standard maintenance and validation procedures, due to their role in the day-to-day follow-up of air pollution episodes, as well as in the long term evaluation of air quality policies (Koutrakis *et al.,* 2001). Technical details on the network and measuring instruments can be found in Jorquera (2002).

For comparison with ceilometer data we have chosen a PM_{10} index constructed as the simple average of the concentrations measured at the six stations mentioned above. Although individual stations show some differences among them, they share similar diurnal and seasonal PM_{10} patterns, so that their average can be considered a robust indicator of the particulate matter concentrations above the city. Fig. 3(a) illustrates the diurnal and seasonal cycles of this PM_{10} index. The days used to construct this figure are not the full period of record, but only 877 days for which ceilometer data are considered (see next section). Still, Fig. 3(a) provides a clear picture of the "climatology" of the PM_{10} problem of Santiago. The diurnal pattern of concentrations is characterized by two conspicuous peaks in the morning and evening. They are related to the morning and evening transitions of the atmospheric boundary layer, when high emission rates combine with a small dispersive capacity of the atmosphere (Muñoz, 2011). In terms of seasonal variation, PM_{10} is definitely a fall-winter problem due to the longer nights and the reduced solar radiation availability required to induce diurnal ventilation of the atmospheric pollutants in the basin. Fig. 3(b) shows the day-to-day variability of 24-hour averaged PM_{10} concentrations. The strong seasonal cycle is again evident, together with large daily variability. The Chilean standard for 24-hour PM_{10} averages (150 $\mu g/m^3$) is rather frequently surpassed in fall and winter.

Ceilometer Data

A Vaisala CL31 ceilometer operates since March 2007 over the roof (~15 m AGL) of the DGF building close to downtown Santiago (point labeled "ce" in Fig. 2). A technical description of the CL31 can be found in Münkel *et al*. (2007). Its setup in Santiago provides mean profiles of range-corrected attenuated backscatter (in units of $1/(10^5 \cdot srad \cdot km)$, hereafter referred to as backscatter units, bu) every 4 to 8 s with vertical resolution of 20 m. We discard in the analysis the first two data levels because they show apparently un-physical high values. Similar measure was taken by Sundström *et al*. (2009) and van der Kamp and McKendry (2010a), the latter mentioning that more recent versions of the CL31 firmware have corrected this problem. In the vertical, the analysis is limited up to 1000 m above the ground, and in time the profiles are averaged over 30-minute periods.

The ceilometer data analyzed covers the overall period from 6 March 2007 to 7 July 2011, although there are periods in which the instrument did not operate, or was moved outside of Santiago basin. Additionally, we have excluded days with rain or substantial fog or low-level clouds,

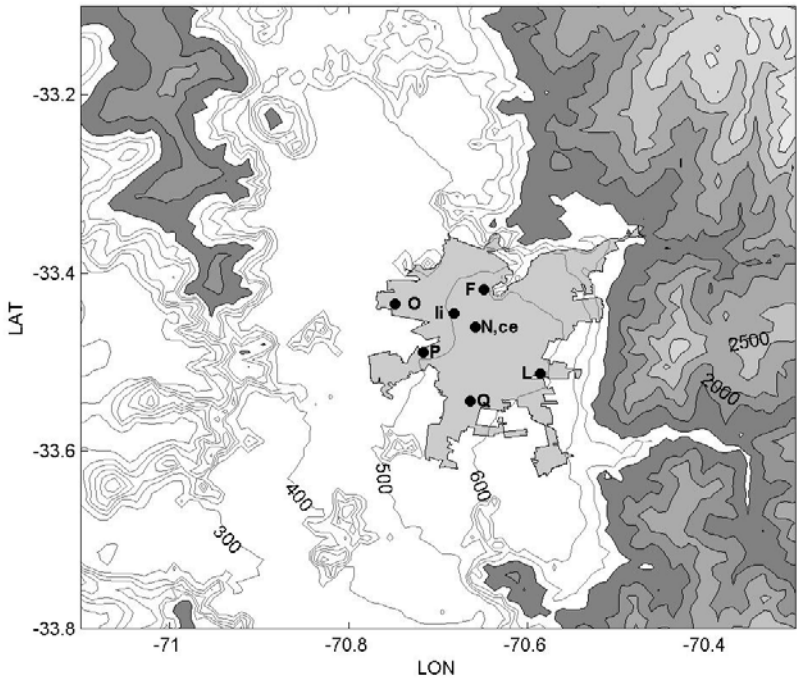

Fig. 2. Topography of Santiago Basin and location of measuring points. Stations F, L, N, O, P, Q belong to the PM_{10}-measuring air pollution monitoring network. Points marked "li" and "ce" (very close to station N) mark locations of lidar and ceilometer instruments, respectively. Terrain heights are contoured from 300 to 800 m above mean sea level (MSL) every 100 m. From 1000 to 3500 m MSL, shade contours are shown every 500 m. Gray shaded zone marks the Santiago metropolitan urban area.

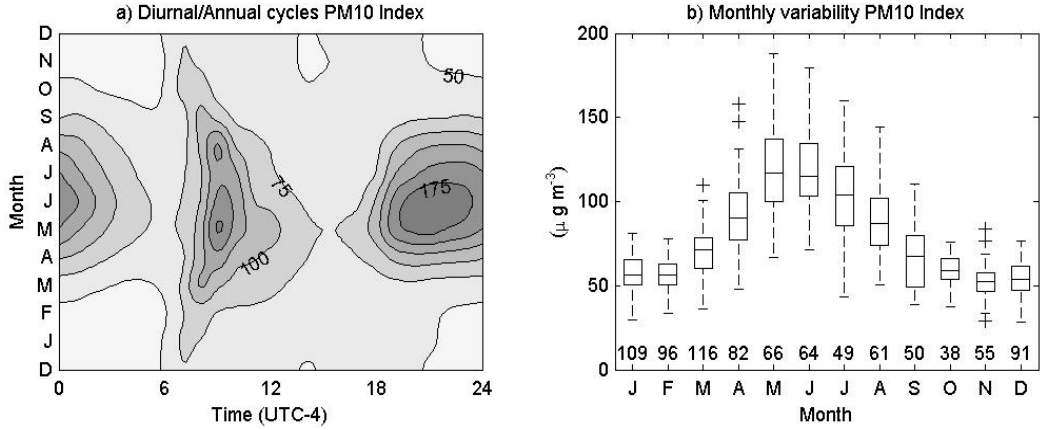

Fig. 3. a) Diurnal/annual cycle diagram of PM_{10} concentrations ($\mu g/m^3$, contours every $25\mu g/m^3$) averaged for the 6 monitoring stations shown in Fig. 2. Time averages are computed for the same 877 days for which ceilometer data are considered, b) Monthly boxplot distributions of daily PM_{10} index. Rectangular boxes extend between the lower and upper quartiles of each distribution, and horizontal lines inside the boxes mark the location of the median. Vertical segmented lines outside the boxes show the extent of the data. Data points lying farther than 1.5 times the interquartile range from the upper or lower quartile are considered outliers and plotted individually with a cross. The numbers at the base of the plot indicate the total number of days considered for each month.

leaving in the analysis 877 days with data (Fig. 3(b) shows the number of days considered for each month). Still, the days remaining in the database include few hours with clouds at some levels, which must be handled cautiously because of the very large backscatter values they present, and which may contaminate the averages. After analysis of the frequency distribution of backscatter values, we decided to replace all values greater than 500 bu with this maximum value. This replacement affects less than 0.02% of the final database.

Lidar Data

The Chilean Weather Service (DMC) has recently acquired a Raymetrics elastic lidar model LB10-ESS-D200. It emits laser pulses at 355 nm wavelength with a repetition rate of 20 Hz. Return signals are available as 30 s averages with 7.5 m vertical resolution. More details of a similar instrument including a comparison with a CL31 ceilometer can be found in Tsaknakis *et al*. (2011). The instrument has been in operation mostly in a 08–24 (UTC-4) mode, beginning on 3 May 2011, in a location about 2.5 km northwest of the ceilometer (point labeled "li" in Fig. 2). We present here lidar observations in terms of its range corrected signal (RCS), and other lidar-derived variables computed by its accompanying analysis software.

CEILOMETER OBSERVATIONS

Diurnal and Seasonal Variation

The diurnal and seasonal variation of the vertical distribution of aerosols over Santiago is illustrated by Fig. 4. Each panel shows 3-month averages of ceilometer backscatter values. The most prominent feature is the diurnal cycle characterized by a deepening of the aerosol layer that starts in the early morning and reaches maximum depth in mid-afternoon. Night-time near-surface backscatter is weak in the spring and summer, contrasting to the high mean values in the fall and winter. The depth of the daytime aerosol layer is appreciably smaller in fall and winter, consistent with the climatology of daytime mixed layer heights derived by Muñoz and Undurraga (2010) using 2 years of this ceilometer data. A secondary maximum in backscatter that appears at hour ~20 at ~500 m in the fall and winter composites will be shown later to mark the occurrence of complex aerosol layers that frequently appear above the site during the evening transition of Santiago's ABL.

Another look at the diurnal/seasonal variation of ceilometer backscatter is presented in Fig. 5(a). Based on the backscatter data for the third ceilometer range level (nominal 40-m height) we construct a diurnal/annual cycle diagram similar to that for PM_{10} presented in Fig. 3(a). Comparison of both figures shows similarities in terms of the maximum values occurring in the morning and in the months of May–June. The monthly distributions of 24-hour averages of backscatter values at 40m shown in Fig. 5(b) present also a similar seasonal pattern as the corresponding distributions of PM_{10} in Fig. 3(b). There are also differences, however, between backscatter and PM_{10} patterns. In particular, Fig. 3(a) shows that backscatter at 40 m has a less marked evening peak as compared to that of PM_{10} concentrations, and there exist also a few hours of phase shift between PM_{10} and backscatter peaks. These differences may be due to the different heights associated to each variable. Panel c) shows the diurnal/annual diagrams of backscatter for the ceilometer level at 300m above the ground. At this height the "morning" peak occurs later in the day when the ABL height surpasses this height, and the evening peak is much less marked than at 40 m. These observations suggest that the evening peak of PM_{10} concentrations is manifestation of a quite shallow aerosol layer near the surface. Fig. 5(d) shows the further decrease in backscatter intensities with height, while at the same time highlighting the secondary evening maximum of backscatter that occurs at these heights in the fall.

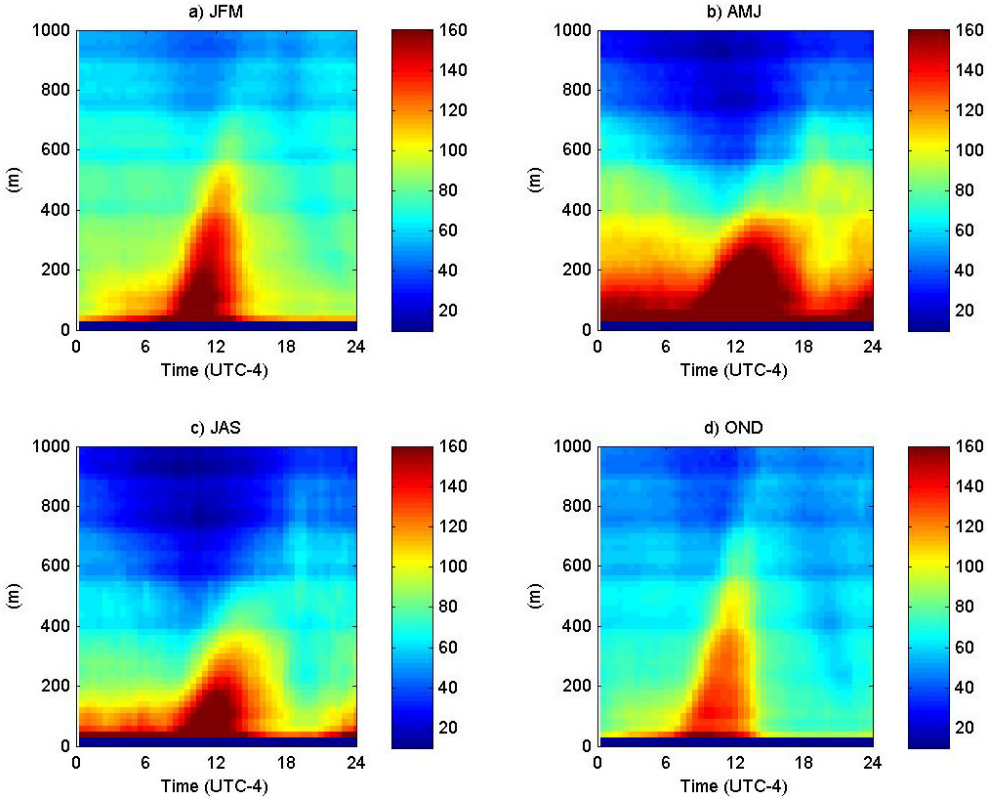

Fig. 4. Time/height averages of ceilometer backscatter intensities (bu) for 3-month periods. a) January–March, b) April–June, c) July–September, d) October–December.

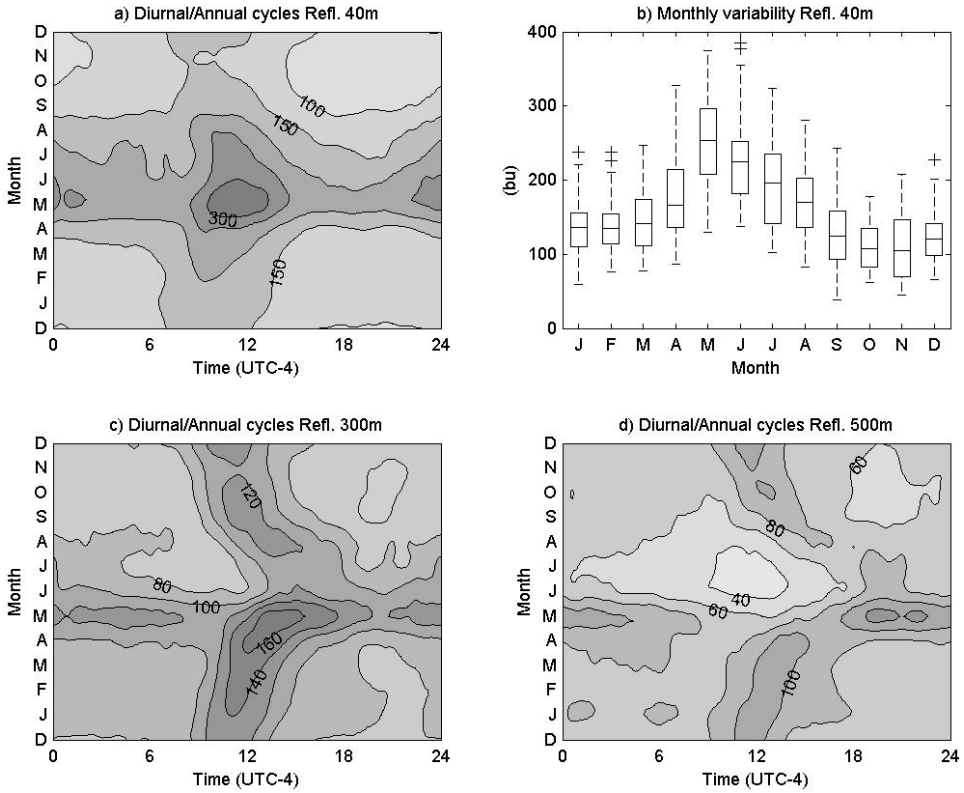

Fig. 5. a) Diurnal/annual cycle diagram of ceilometer backscatter intensity (b.u., contours every 50 bu) for the ceilometer data level at 40 m above the surface, b) Monthly boxplot distributions of daily averages of 40 m-ceilometer backscatter intensities, c) As a) but for 300 m above the surface, d) As a) but for 500 m above the surface. Gray-scales in c) and d) are different than in a).

Relationship with PM_{10}

The previous analysis showed that surface PM_{10} and ceilometer backscatter values are well related in terms of their mean diurnal and annual cycles. We quantify now their co-variability at inter-daily scales. For this purpose we have defined for each month groups of high and low PM_{10} values based on the upper and lower quartiles of the monthly distributions of the 24-hour averaged PM_{10} index. Next, we averaged the ceilometer backscatter values for the high-PM_{10} and low-PM_{10} days independently. Finally, we computed the differences of these two averages. In order to assign a statistical significance to these differences, we performed a simple Monte Carlo test. For each month we selected random groups of days of the same size as the high-PM_{10} and low-PM_{10} groups and computed differences of their averages. By performing 1000 of these experiments, we generated a statistical distribution of differences for each hour and level. The significance of the high-PM_{10}/low-PM_{10} differences is evaluated in terms of this distribution.

Fig. 6 shows the results grouped in 3-month panels. Vertical regions and time periods in which the differences are positive (negative) are those for which backscatter is larger (smaller) in high-PM_{10} days as compared to low-PM_{10} days. As could be expected, below 400 m AGL most differences are positive and significant to 90%. In fall and winter the largest backscatter differences define a region that grows in depth starting very shallow in the morning and reaching maximum vertical extent in the afternoon transition. Interestingly, the differences are non-significant or even negative by the end of the night and above the growing high-difference layer. One interpretation of this observation is that high-PM_{10} days are mainly driven by near-surface emissions and stability, and that the air at ~500 m AGL, above the growing ABL, may be even cleaner in high-PM_{10} days than in low-PM_{10} days. Synoptic analysis of Santiago's air pollution problem has shown indeed that during PM_{10} episodes the regional subsidence is stronger (Rutllant and Garreaud, 1995), which may be associated to a cleaner and drier (but more stable) air mass aloft. In spring and summer, on the other hand, the backscatter differences are smaller but more homogeneously positive over all the lowest 500 m AGL.

Another way of quantifying the relationship between ceilometer backscatter and PM_{10} concentrations is through the computation of linear correlation coefficients. Care has to be taken of the strong mean seasonal cycle of both variables, which must be filtered out before computing the correlations. For that purpose, we computed first the monthly anomalies of each variable with respect to their monthly averages. Fig. 7(a) shows the scatter diagram between the monthly anomalies of PM_{10} and the 40-m backscatter values for all 877 points of the database. Fig. 7(b) shows the vertical profiles of correlation coefficients built by considering the different ceilometer data levels. Maximum correlation is

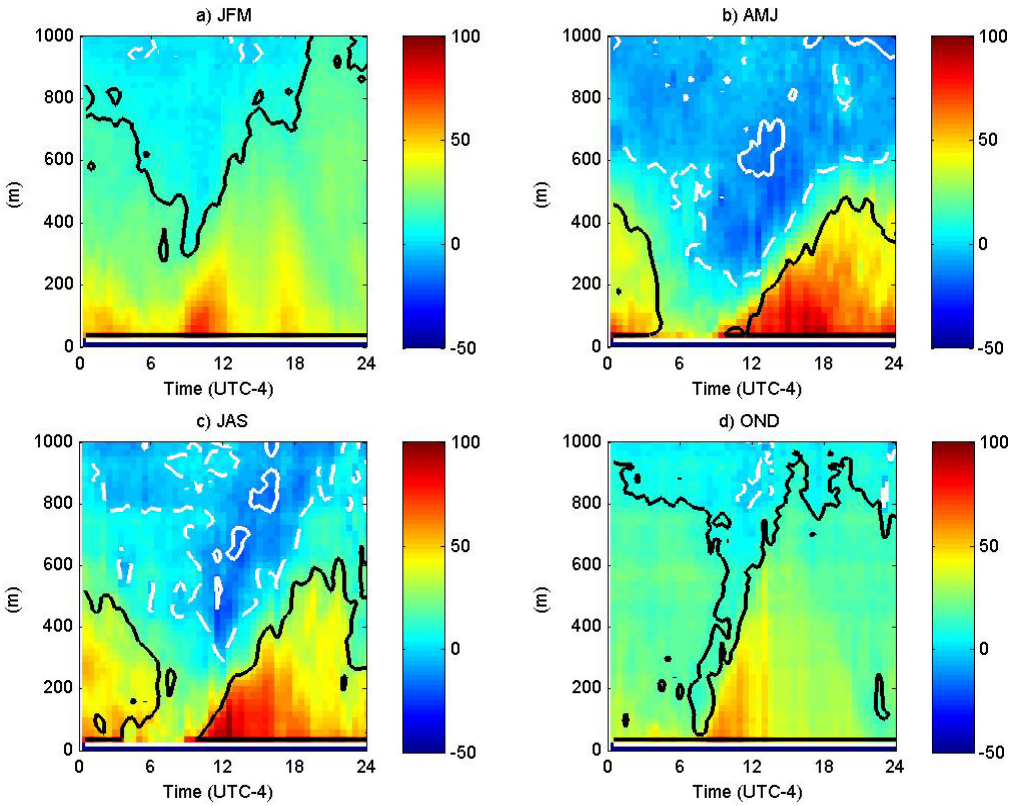

Fig. 6. Time/height diagrams of the differences between ceilometer backscatter intensities (b.u.) for high-PM_{10} and low-PM_{10} days. Dashed white contour marks the zero value. Black and white bold contours define regions where the differences are significant to 90% according to a Monte Carlo test (see text). a) January–March averages, b) April–June averages, c) July–September averages, d) October–December averages.

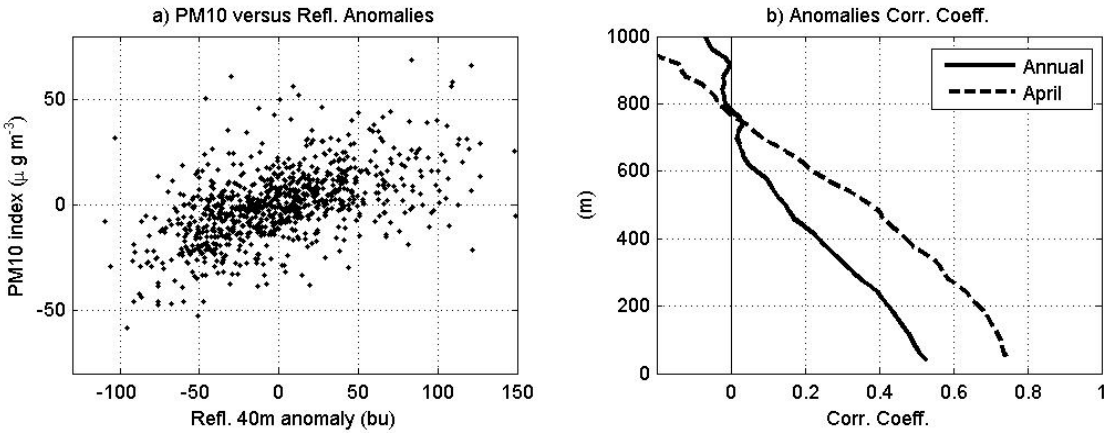

Fig. 7. a) Scatter diagram between PM_{10} index and ceilometer backscatter intensities at 40 m. Values correspond to anomalies with respect to monthly averages. b) Vertical profiles of correlation coefficient between anomalies of PM_{10} index and ceilometer backscatter intensities. Continuous line corresponds to all data. Dashed line corresponds to April anomalies.

found near the surface with r ~0.5 for the full data set, and r ~0.75 for April. Van der Kamp and McKendry (2010b) reported a 0.45 correlation coefficient between ceilometer backscatter and PM_{10} concentrations using data of 14 vertical profiles measured during one night over Vancouver, Canada, while Münkel *et al*. (2004; 2007) report correlation coefficients ~0.8 in the comparison of 5736 half-hourly averages of PM_{10} and ceilometer backscatter intensities measured in Hanover, Germany. Half-hourly time series and one-night vertical profiles, however, may have larger autocorrelations than the daily averages used in the present study, so that correlation values are not directly comparable. Our results, nonetheless, confirm the conclusions of these other studies with respect to the ability of ceilometers to characterize particulate matter distribution in the ABL.

LIDAR OBSERVATIONS

The lidar operated continuously from 23 to 28 June 2011 during the development of an air pollution episode. Fig. 8 presents ceilometer and lidar observations for 24 June 2011. Panel a) shows the ceilometer backscatter field which clearly marks the growing of the convective boundary layer from hours 09 to 14. After hour 14 the intensity of the near surface decreases, although hints of continuous ABL growth can be perceived up to ~15:30. After that time the backscatter below 400 m decreases sharply, although high values are still observed in the 400–800 m layer. After hour 20 a near surface high-backscatter layer develops. Panels b) and c) show lidar-derived variables. Panel b) corresponds to the lidar range corrected signal (RCS), and panel c) shows the aerosol backscatter coefficient. The RCS clearly shows the development of the aerosol layers above 500 m that appear during the evening transition. Below 500 m, however, the more homogeneous large values of the RCS make it more difficult to appreciate the evolution of the aerosol layer, as compared to the ceilometer field. The structure of the lidar-derived aerosol backscatter shown in panel c), on the other hand, compares better with the ceilometer field. During daytime, the growth of the convective ABL is more apparent in this plot than in panel b). In the evening transition, also, the distinction between the high values aloft and low signal below is similar to that of the ceilometer. The lidar backscatter values, however, show some fine scale noise (very clear around midday) which may be due to its computation algorithm. Differences in the lidar RCS and aerosol backscatter fields originate mainly in the inclusion of the molecular backscatter in the former variable. At the 355 nm lidar wavelength, the effect of molecular backscatter is much larger as compared to its effect in the 905 nm wavelength of the ceilometer.

The appearance of elevated aerosol layers during the evening transition is something that ceilometer data suggests as a rather frequent phenomenon, but that now lidar observations confirm. For the particular day of Fig. 8, and as part of efforts to monitor the development of the air pollution episode, DMC launched three radiosondes from the lidar site in the morning, around midday, and in the evening. Fig. 9 shows the corresponding temperature, water vapor mixing ratio, and wind profiles from the surface up to 2000 m. In addition, panel d) shows the corresponding average profiles of the lidar RCS. The evening peak at ~800 m in this last panel marks well the elevated aerosol layer. It is clearly associated to a water vapor peak that appears at the same time and height (panel b). All this development occurs in a near isothermal region (panel a) between ~500 and 1200 m, which shows also weak winds, probably due to the topographical confinement of the basin. The large aerosol content of the elevated layers and their water vapor mixing ratio values suggest that they could be originally near-surface air layers that at this time of the day have become detached and arrive at the site as elevated aerosol layers. An alternate explanation could be aerosol growth by moisture uptake as postulated by Emeis *et al.* (2011) to explain detached ceilometer backscatter maximums in a nocturnal ABL. In their case, however, relative humidities were ~90%, while in this case the detached peak in relative humidity reaches only 56% (fine dotted line in Fig. 9(b)). As mentioned earlier, these complex evening transitions are rather frequent in the fall, as illustrated by

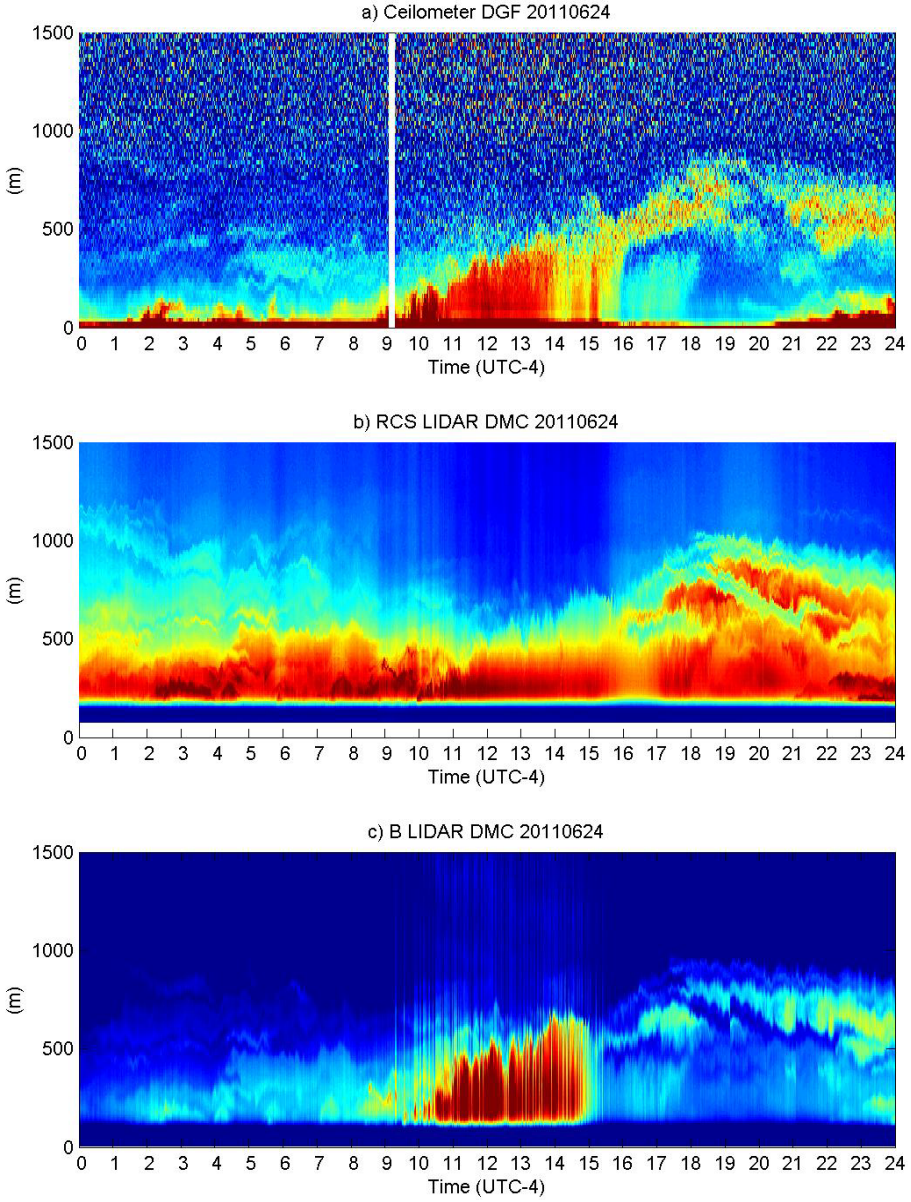

Fig. 8. Data for 24 June 2011. a) Ceilometer backscatter intensities, b) Lidar range corrected signal, c) Lidar aerosol backscatter.

the four examples shown in Fig. 10. They correspond also to the features leaving a secondary maximum in the ceilometer averaged backscatter fields noted previously in Fig. 4. The precise dynamics and spatial structure of this phenomenon have not been studied yet, but it may be of importance for the air pollution problem of Santiago. Dwelling into this problem, however, falls beyond the scope of this paper and warrants further study.

Another phenomenon that the lidar has shown is the frequent occurrence of buoyancy oscillations in the lower troposphere over Santiago. This phenomenon is best visualized by means of the lidar-derived variable fdfLR, defined as a smoothed derivative of the smoothed natural logarithm of the RCS (Fig. 11). The aerosol layers in the stable basin's air mass show often periods with quasi-harmonic height variation in time. They are most frequently observed near the surface in the morning (Fig. 11(a)) and in the residual boundary layer in the evening transition (Fig. 11(b)). The most dramatic case up to now is shown in Fig. 11(c), covering almost 6 hours during the evening transition on 23 May 2011. Several layers of aerosol showing oscillations of various amplitudes during the full period can be observed in Fig. 11(c). We call them buoyancy oscillations, because their periods (~5 minutes) are similar to the Brunt-Väisälä period of a near isothermal atmospheric layer. What is especially remarkable of the oscillations in Fig. 11(c) is their large amplitude, reaching almost 500 m at ~19:15 in the layer at ~2000 m AGL. In this particular case the amplitude and pulse duration increase significantly with height, as clearly seen in the 18:00 and 19:00 pulses. This observation suggests that the source level of the oscillations may have been aloft. Further study of the forcing and dynamics of these oscillations is left for future research.

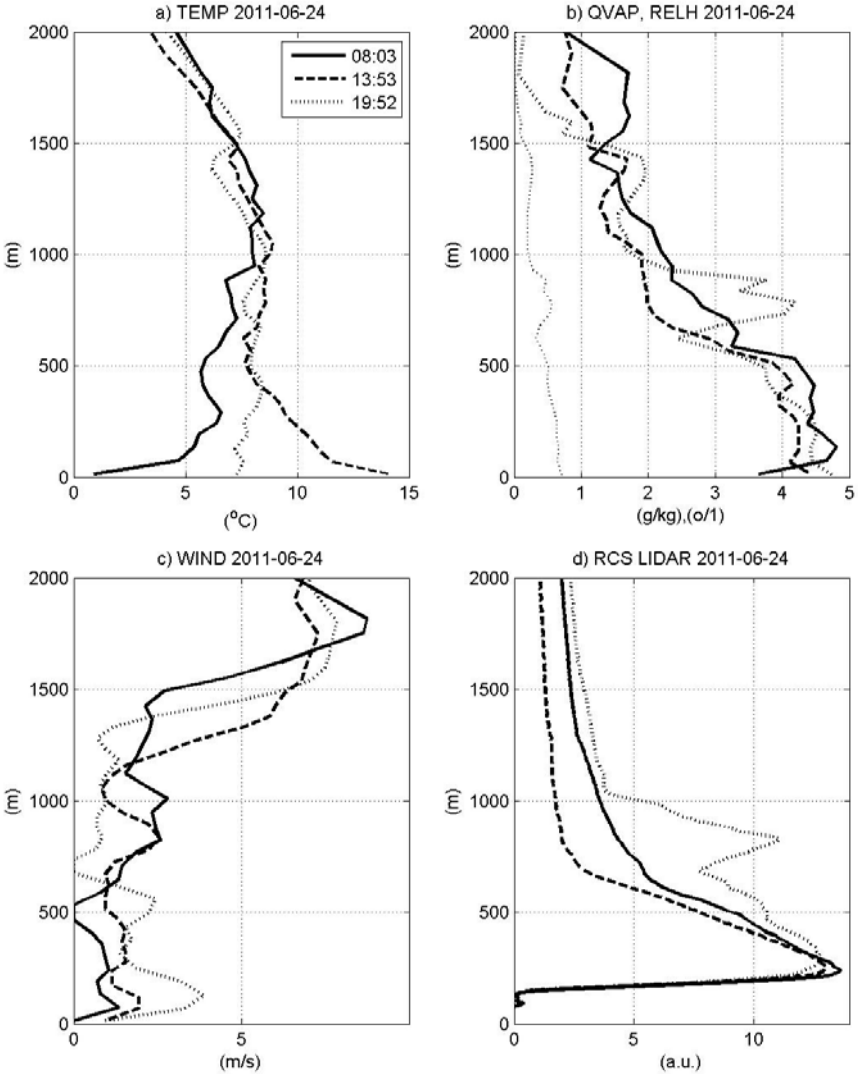

Fig. 9. Vertical profiles measured on 24 June 2011 with radiosondes and lidar . a) Temperature, b) water vapor mixing ratio (bold lines) and relative humidity (fine dotted line for time 19:52 UTC-4 in unit fractions), c) wind speed, d) Lidar range corrected signal (1-hour averages around each time). Times (UTC-4) are shown in panel a).

CONCLUSIONS

This paper has described new observations gathered in Santiago (Chile) with two recently available lidar instruments. The large aerosol load of Santiago basin's air mass makes the application of lidars useful for improving the characterization of its severe air pollution problem, as well as for providing a new look of Santiago's atmospheric boundary layer dynamics. A total of 877 days of half-hourly ceilometer backscatter profiles was used to describe the diurnal and seasonal variation of the vertical distribution of aerosols over Santiago. Large diurnal variation of backscatter values is observed on average up to heights ~600 m in spring and summer, and ~400 m in fall and winter. During the cold season, average backscatter intensities in the lowest ceilometer levels are much larger as compared with the warm season, consistent with the near-surface PM_{10} climatology. A secondary maximum of backscatter intensities appears in the fall and winter average backscatter fields during the evening transition, which appears related to the frequent development of complex aerosol layers over the site at this time of the day. Comparison of ceilometer backscatter and PM_{10} concentrations shows that in terms of their diurnal pattern, both show prominent morning peaks, which in the ceilometer data is weaker and occurs later with height above the ground. The evening peak, on the other hand, which is the most important feature in the surface PM_{10} diurnal cycle, is only weakly shown in ceilometer backscatter, suggesting that this significant aspect of Santiago's air pollution problem is constrained to a rather shallow atmospheric layer. In fact, comparison of mean ceilometer backscatter values for high-PM_{10} versus low-PM_{10} suggests that during PM_{10} episodes in the fall and winter, aerosol loads above ~400 m AGL may be lower than during non-episode days. Further comparison of ceilometer backscatter with PM_{10} concentrations was accomplished by computation of correlation coefficients between their daily anomalies with respect to monthly

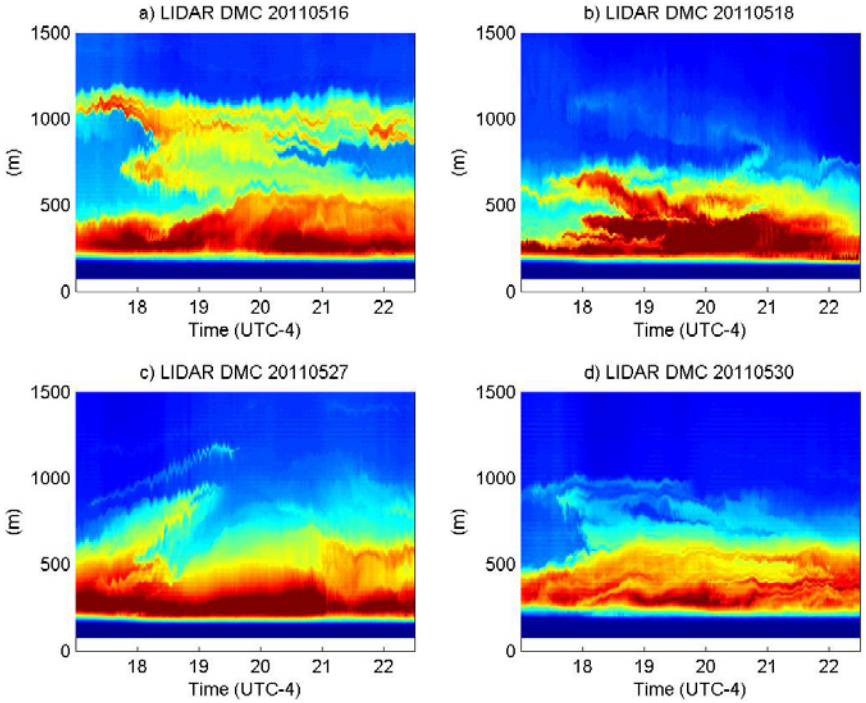

Fig. 10. Lidar range corrected signal during evening transitions (17:00 to 22:30 UTC-4). a) 16 May 2011, b) 18 May 2011, c) 27 May 2011, d) 30 May 2011.

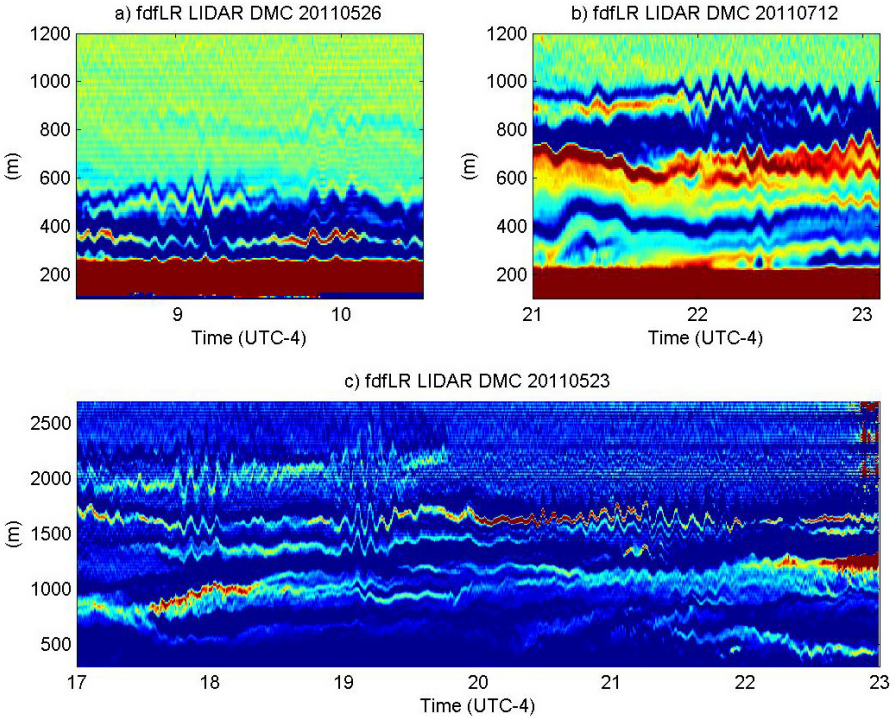

Fig. 11. Vertical/time fields of lidar-derived signal (see text). a) 26 May 2011, b) 12 July 2011, c) 23 May 2011. Color scales in each plot have been adjusted to highlight oscillations.

means. Maximum correlations were found for the lowest ceilometer data level, with r ~0.5 for the full dataset, and a maximum value of r ~0.75 for the month of April. These figures are similar to those obtained elsewhere (Münkel *et al*., 2007; van der Kamp and McKendry, 2010b).

Comparison of ceilometer and lidar observations was performed for a day during a high-PM_{10} episode in June 2011. Due to the ~200 m blind region of the lidar, the ceilometer provides a more complete picture of aerosol layers close to the surface, showing very well the growth

of the convective boundary layer during daytime. Aerosol layers at ~500 m in the residual and stable ABL, on the other hand, are more sharply defined by the lidar, especially through its aerosol backscatter derived variable. Both instruments suggest the frequent development of rather complex aerosol layers appearing over Santiago during the evening transition. These layers may highly increase the integrated load of aerosols over the nocturnal boundary layer, resulting thus of potential significance for the air pollution of Santiago. Investigation of their spatial structure and dynamics is proposed as a relevant problem to address in future studies. Finally, the high resolution of lidar observations has allowed observation of fine details in the dynamics of aerosol layers over Santiago. A frequent phenomenon found is the occurrence in the stable boundary layer of short-period buoyancy oscillations. In one of the cases illustrated here, these oscillations were observed for ~6 hours, and had amplitudes up to 500 m at heights ~2000 m above the ground. Study of the forcing and dynamics of these oscillations is another line of future research suggested by these new observations.

ACKNOWLEDGMENTS

Comments by Drs. Rainer Schmitz, Roberto Rondanelli, Laura Gallardo, and three anonymous reviewers are thanked. Mr. Marcelo Corral from the Ministry for the Environment is thanked for facilitating access to PM_{10} data. The DGF ceilometer was acquired through a Mecesup project led by Dr. René Garreaud.

DISCLAIMER

Reference to any companies or specific commercial products does not constitute endorsement.

REFERENCES

Baxla, S.P., Roy, A., Gupta, T., Tripathi, S.N. and Bandyopadhyaya, R. (2009). Analysis of Diurnal and Seasonal Variation of Submicron Outdoor Aerosol Mass and Size Distribution in a Northern Indian City and its Correlation to Black Carbon. *Aerosol Air Qual. Res.* 9: 458–469.

Cohn, S.A. and Agevine W.M. (2000). Boundary Layer Height and Entrainment Zone Thickness Measured by Lidars and Wind Profiling Radars. *J. Appl. Meteorol.* 39: 1233–1247.

De Wekker, S. and Mayor S. (2009). Observations of Atmospheric Structure and Dynamics in the Owens Valley of California with a Ground-based, Eye-safe, Scanning Aerosol Lidar. *J. Appl. Meteorol. Clim.* 48: 1483–1499.

Emeis, S. (2011). *Surface-based Remote Sensing of the Atmospheric Boundary Layer*, Springer.

Eresmaa, N., Karppinen, A., Joffre, S., Räsänen, J. and Talvitie, H. (2006). Mixing Height Determination by Ceilometer. *Atmos. Chem. Phys*. 6: 1485–1493.

Heese, B., Flentje, H., Althausen, D., Ansmann, A. and Frey, S. (2010). Ceilometer Lidar Comparison: Backscatter Coefficient Retrieval and Signal-to-noise Ratio Determination. *Atmos. Meas. Tech.* 3: 1763–1770.

Jorquera, H. (2002). Air Quality at Santiago, Chile: A Box Modeling Approach. I. Carbon Monoxide, Nitrogen Oxides and Sulfur Dioxide. *Atmos. Environ*. 36: 315–330.

Koutrakis, P., Sax, S., Sarnat, J., Coull, B., Demokritou, P., Oyola, P., García, J. and Gramsch, E. (2001). Analysis of PM_{10}, $PM_{2.5}$, and $PM_{2.5–10}$ Concentrations in Santiago, Chile, from 1989 to 2001. *J. Air Waste Manage. Assoc.* 55: 342–351.

Kovalev, V. and Eichinger, W.E. (2004). *Elastic Lidar*, John Wiley & Sons, Inc. Hoboken, New Jersey, U.S.A.

Martucci, G., Matthey, R. and Mitev, V. (2007). Comparison between Backscatter Lidar and Radiosonde Measurements of the Diurnal and Nocturnal Stratification in the Lower Troposphere. *J. Atmos. Oceanic Technol.* 24: 1231–1244.

McKendry, I., Strawbridge, K. and Jones, A. (2011). Continuous 1064/532 nm Lidar Measurements (CORALNet-UBC) in Vancouver, British Columbia: Selected Results from a Year of Operation. *Atmos. Ocean* 49: 32–40.

McKendry, I., Van der Kamp, D., Strawbridge, K., Christen, A. and Crawford, B. (2009). Simultaneous Observations of Boundary-layer Aerosol Layers with CL31 Ceilometer and 1064/532 nm Lidar. *Atmos. Environ*. 43: 5847–5852.

Molina, M. and Molina, J. (2004). Megacities and Atmospheric Pollution. *J. Air Waste Manage. Assoc.* 54: 644–680.

Münkel, C., Emeis, S., Müller, W.J. and Schäfer, K.P. (2004). In *Remote Sensing of Clouds and the Atmosphere VIII*, Schäfer K., Comerón, A., Carleer, M.R. and Picard R.H. (Eds.), *Proc. SPIE* 5235: 486–496 Bellingham, WA, doi: 10.1117/12.511104.

Münkel, C., Eresmaa, N., Räsänen, J. and Karppinen, A. (2007). Retrieval of Mixing Height and Dust Concentration with Lidar Ceilometer. *Boundary Layer Meteorol* 124: 117–128.

Muñoz, R. (2011). Relative Roles of Emissions and Meteorology in the Diurnal Pattern of Urban Particulate Matter: Analysis of the Daylight Saving Time Effect. Submitted to *J. Air Waste Manage. Assoc.*

Muñoz, R. and Corral, M. (2011). Comparison of the Vertical Structure of the Atmosphere over Santiago and Santo Domingo: Preliminary Results (in Spanish), 2nd Congress on Physical Oceanography, Meteorology and Climate of the Southeast Pacific, La Serena, Chile, 5–7 October, 2011.

Muñoz, R. and Undurraga, A. (2010). Daytime Mixed Layer over the Santiago Basin: Description of Two Years of Observations with a Lidar Ceilometer. *J. Appl. Meteorol. Clim*. 49: 1728–1741.

Papayannis, A., Zhang, H.Q., Amiridis, V., Ju, H.B., Chourdakis, G., Georgoussis, G., Pérez, C., Chen, H.B., Goloub, P., Mamouri, R.E., Kazadzis, S., Paronis, D., Tsaknakis, G. and Baldasano, J.M. (2007). Extraordinary Dust Event over Beijing, China, during April 2006: Lidar, Sun Photometric, Satellite Observations and Model Validation. *Geophys. Res. Lett*. 34: L07806, doi:

10.1029/2006GL029125.

Ponczkowska, A., Zielinski, T., Petelski, T., Markowicz, K., Chourkadis, G. and Georgoussis, G. (2009). Aerosol Optical Depth Measured at Different Coastal Boundary Layers and its Links with Synoptic-scale Features. *Remote Sens*. 1: 557–576.

Rana, S., Kant, Y. and Dadhwal, V.K. (2009). Diurnal and Seasonal Variation of Spectral Properties of Aerosols over Dehradun, India. *Aerosol Air Qual. Res.* 9: 32–49.

Romero, H., Ihl, M., Rivera, A. and Zalazar, P. (1999). Rapid Urban Growth, Land-use Changes and Air Pollution in Santiago, Chile. *Atmos. Environ*. 33: 4039–4047.

Rutllant, J. and Garreaud, R. (1995). Meteorological Air Pollution Potential for Santiago, Chile: Towards an Objective Episode Forecasting. *Environ. Monit. Assess*. 34: 223–244.

Saide, P., Carmichael, G., Spak, S., Gallardo, L., Osses, A., Mena, M. and Pagowski, M. (2011). Forecasting Urban PM_{10} and $PM_{2.5}$ Pollution Episodes in very stable Nocturnal Conditions and Complex Terrain Using WRF-Chem CO Tracer Model. *Atmos. Environ*. 45: 2769–2780.

Schmitz, R. (2005). Modelling of Air Pollution Dispersion in Santiago de Chile. *Atmos. Envir*on. 39: 2035–2047.

Sundström, A.M., Nousiainen, T. and Petäjä, T. (2009). On the Quantitative Low-level Aerosol Measurements using Ceilometer-type Lidar. *J. Atmos. Oceanic Technol.* 26: 2340–2352.

Tsaknakis, G., Papayannis, A., Kokkalis, P., Amiridis, A., Kambezidis, H., Mamouri, R., Georgoussis, G. and Advikos, G. (2011). Inter-comparison of Lidar and Ceilometer Retrievas for Aerosol and Planetary Boundary Layer Profiling over Athens, Greece. *Atmos. Meas. Tech*. 4: 1261–1273.

Van der Kamp, D. and McKendry, I. (2010a). Diurnal and Seasonal Trends in Convective Mixed-layer Heights Estimated from Two Years of Continuous Ceilometer Observations in Vancouver, BC. *Boundary Layer Meteorol.* 137: 459–475.

Van der Kamp, D. and McKendry, I. (2010b). Comparison of Tethered Balloon Vertical Profiles of Particulate Matter Size Distributions with Lidar Ceilometer Backscatter in the Nocturnal Urban Boundary Layer. *Int. J. Environ. Pollut*. 41: 155–165.

World Bank (2010). *World Development Indicators*, World Bank, New York.

Received for review, August 22, 2011
Accepted, October 25, 2011